Tomáš Marhan; Petr Sváček

Numerical approximation of aeroacoustics induced by flow over a square cylinder

In: Jan Chleboun and Jan Papež and Karel Segeth and Jakub Šístek and Tomáš Vejchodský (eds.): Programs and Algorithms of Numerical Mathematics, Proceedings of Seminar. Hejnice, June 23-28, 2024. Institute of Mathematics, Czech Academy of Sciences, Prague, 2025. pp. 115–126.

Persistent URL: http://dml.cz/dmlcz/703226

Programs and Algorithms of Numerical Mathematics 22
J. Chleboun, J. Papež, K. Segeth, J. Šístek, T. Vejchodský (Eds.)
Institute of Mathematics CAS, Prague 2025

NUMERICAL APPROXIMATION OF AEROACOUSTICS INDUCED BY FLOW OVER A SQUARE CYLINDER

Tomáš Marhan, Petr Sváček

Department of Technical Mathematics, Faculty of Mechanical Engineering,
Czech Technical University in Prague
Technická 4, 166 01 Prague 6, Czechia
tomas.marhan@fs.cvut.cz, petr.svacek@fs.cvut.cz

Abstract: This study investigates the generation of aeroacoustic sound resulting from the interaction of flow with a square cylinder at a Reynolds number of 150 and a Mach number of 0.2. The analysis combines the Finite Volume Method (FVM) for fluid dynamics using the OpenFOAM framework with the Finite Element Method (FEM) for acoustics implemented via the FEniCS Python library.

Keywords: finite element method, finite element method, aeroacoustic, OpenFOAM, FEniCS, CFD, CAA

MSC: 76Q05

1. Introduction

For many years, Computational Fluid Dynamics (CFD) has been widely used across various scientific and industrial fields. With recent advancements in computational resources, it has become feasible to study also flow-induced noise from bluff bodies, such as the noise generated by aircraft landing gear or car side mirrors.

Aeroacoustics, the study of noise generated and propagated by fluid flows, poses a unique challenge because the sound pressure is much smaller than the atmospheric pressure. Moreover, as the Mach number decreases, the disparity between the fluid length scale and the acoustic length scale (wavelength) increases. Consequently, the mesh size required to resolve fluid length scales becomes significantly smaller than that needed for acoustic length scales. To address this, a variety of Computational Aeroacoustics (CAA) methodologies have been adopted, many of which separate the flow field from the acoustic computation in a hybrid approach (see [7] for an overview). The aim is to derive the equations that describe the generation of sound waves propagating into the acoustic field, separately from those that define fluid motion in the unsteady flow. The hybrid approach has been successfully applied in cases like low Mach airframe noise in [4] and human phonation in [8].

DOI: 10.21136/panm.2024.11

This study focuses on low Mach number laminar air flow over a square cylinder, a classical problem in fluid mechanics with practical relevance to building design. The interaction between the flow and the body leads to vortex shedding, forming a von Kármán vortex street that generates acoustic waves. The investigation of acoustic emissions is conducted using a combination of two open-source tools, OpenFOAM and FEniCS. The integration of these tools is detailed in Chapter 5.

2. The mathematical model

We consider the conservation of mass equation and the conservation of momentum equation given by

$$\frac{\partial \rho}{\partial t} + \nabla \cdot (\rho\, \mathbf{u}) = 0\,, \tag{1}$$

$$\frac{\partial (\rho\, \mathbf{u})}{\partial t} + \nabla \cdot (\rho\, \mathbf{u} \otimes \mathbf{u} - \boldsymbol{\sigma}) = 0\,, \tag{2}$$

where $\mathbf{u}$ denotes the fluid velocity, ρ fluid density and t time. For fluid, the stress tensor $\boldsymbol{\sigma}$ is defined as

$$\boldsymbol{\sigma} = -p\, \mathbf{I} + \boldsymbol{\tau}\,, \tag{3}$$

where p is static pressure, $\boldsymbol{\tau}$ denotes the viscous (shear) stress tensor and $\mathbf{I}$ is the unit tensor. Since air is a Newtonian fluid, the constitutive relation between the viscous stress tensor and the rate of strain tensor is expressed as

$$\boldsymbol{\tau} = \mu \left(\nabla \mathbf{u} + (\nabla \mathbf{u})^T \right) - \frac{2}{3} \mu \nabla \cdot \mathbf{u}\,, \tag{4}$$

where μ is dynamic viscosity of the fluid. At low Mach numbers, the fluid is assumed to be nearly incompressible, implying that the density remains constant and the velocity field is divergence-free.

In order to obtain unique solution for eq. (1) and (2) we have to consider bounded domain $\Omega_1 \subset \mathbb{R}^2$ with boundary conditions defined on Lipschitz boundary $\partial\Omega_1$. The boundary $\partial\Omega_1$ is further subdivided as $\partial\Omega_1 = \Gamma_\mathrm{b} \cup \Gamma_1$ and $\Gamma_1 = \Gamma_\mathrm{in} \cup \Gamma_\mathrm{out} \cup \Gamma_\mathrm{slip}$, as illustrated in Fig. 1.

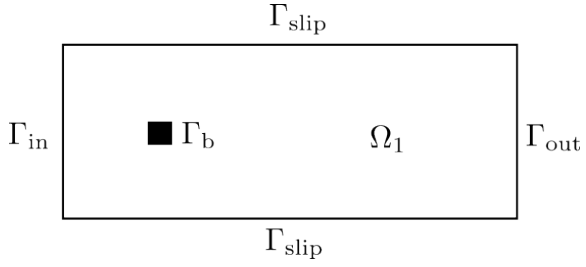

Figure 1: Fluid computational domain.

The initial-boundary value problem for incompressible fluid is then formulated as: for $t \in (0,T]$ find $\mathbf{u}(\mathbf{x},t) : \Omega_1 \times (0,T] \to \mathbb{R}^2$ and $p(\mathbf{x},t) : \Omega_1 \times (0,T] \to \mathbb{R}$ such that

$$\begin{aligned} \frac{\partial \mathbf{u}}{\partial t} + \nabla \cdot (\mathbf{u} \otimes \mathbf{u}) - \nabla \cdot (\nu \nabla \mathbf{u}) + \frac{1}{\rho_0} \nabla p = \mathbf{0} \quad & \text{in } \Omega_1 \times (0,T] \,, \\ \nabla \cdot \mathbf{u} = 0 \quad & \text{in } \Omega_1 \times (0,T] \,, \end{aligned} \tag{5}$$

where ν is the kinematic viscosity (dynamic viscosity divided by density) of the fluid and ρ_0 is the freestream density. The boundary and initial conditions are prescribed as follows

$$\begin{aligned} \mathbf{u} &= \mathbf{0} && \text{on } \Gamma_\mathrm{b} && \times (0,T] \,, \\ \mathbf{u} &= (U_\infty, 0) && \text{on } \Gamma_\mathrm{in} && \times (0,T] \,, \\ -\nu \frac{\partial \mathbf{u}}{\partial \mathbf{n}} + \frac{p}{\rho_0} \mathbf{n} &= \mathbf{0} && \text{on } \Gamma_\mathrm{out} && \times (0,T] \,, \\ \mathbf{u} \cdot \mathbf{n} &= 0 && \text{on } \Gamma_\mathrm{slip} && \times (0,T] \,, \\ \frac{\partial p}{\partial \mathbf{n}} &= 0 && \text{on } \Gamma_1 \setminus \Gamma_\mathrm{out} \cup \Gamma_\mathrm{b} && \times (0,T] \,, \\ \mathbf{u}(\mathbf{x},0) &= (U_\infty, 0) && \text{for } \mathbf{x} \in \Omega_1 \,, \end{aligned} \tag{6}$$

where U_∞ is the freestream velocity and $\mathbf{n}$ is the outward unit vector to Γ_b and Γ_1.

Aeroacoustics

The most widely used CAA formulation is Lighthill's aeroacoustic analogy, where the governing equations (1) and (2) are reformulated into a wave-like equation, as detailed in [5]. In this approach, acoustic noise is radiated from a localized region of fluctuating flow embedded within an infinite homogeneous fluid, see Fig. 2. In the surrounding fluid, the speed of sound c_0, the density ρ_0 and the pressure p_0 are constants and the density fluctuations $\rho' = \rho - \rho_0$ are governed by the standard homogeneous acoustic wave equation. Within the fluctuating region, the Lighthill's aeroacoustic equation is derived by taking the time derivate of the continuity equation (1) and subtracting the divergence of the momentum equation (2), which yields

$$\frac{\partial^2 (\rho - \rho_0)}{\partial t^2} = \nabla \cdot \nabla \cdot \left[\rho \, \mathbf{u} \otimes \mathbf{u} + (p - p_0) \, \mathbf{I} - \boldsymbol{\tau} \right] , \tag{7}$$

where $p' = p - p_0$ are the pressure perturbations. Further substracting the term $c_0^2 \Delta (\rho - \rho_0)$ from both sides of eq. (7), we retrieve the desired inhomogeneous wave equation

$$\left(\frac{\partial^2}{\partial t^2} - c_0^2 \Delta \right) (\rho - \rho_0) = \nabla \cdot \nabla \cdot \mathbf{T} \,, \tag{8}$$

where the Lighthill's tensor $\mathbf{T}$ is introduced as

$$\mathbf{T} = \rho \, \mathbf{u} \otimes \mathbf{u} + \left[(p - p_0) - c_0^2 (\rho - \rho_0) \right] \mathbf{I} - \boldsymbol{\tau} \,. \tag{9}$$

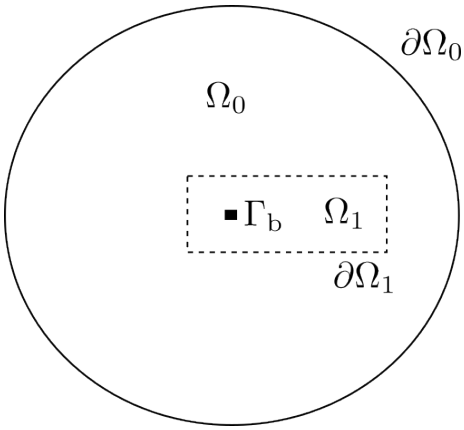

Figure 2: Aeroacoustic computational domain.

The Lighthill's tensor in eq. (9) consists of three terms. The viscous source term $\boldsymbol{\tau}$ is significant only at low Reynolds numbers and over sufficiently long distances, so it is often neglected. Additionally, for low Mach numbers flows and no heat effects, the fluid can be considered isentropic, meaning the relation $p' = c_0^2 \rho'$ holds and density can be approximated by the density of the resting media ρ_0. Under these conditions, the Lighthill's tensor reduces to $\mathbf{T} \approx \rho_0 \, \mathbf{u} \otimes \mathbf{u}$ and eq. (8) results in the following inhomogeneous wave equation

$$\frac{1}{c_0^2} \frac{\partial^2 p'}{\partial t^2} - \Delta p' = \nabla \cdot \nabla \cdot (\rho_0 \, \mathbf{u} \otimes \mathbf{u}) \ . \tag{10}$$

In order to solve eq. (10) we consider the homogeneous fluid region to be finite and bounded. We denote the aeroacoustic computational domain as $\Omega_0 \subset \mathbb{R}^2$ with Lipschitz boundary $\partial\Omega_0$, such that $\Omega_1 \subset \Omega_0$, see Fig. 2. The boundary $\partial\Omega_0$ is further subdivided as $\partial\Omega_0 = \Gamma_\mathrm{b} \cup \Gamma_0$. The initial-boundary value problem then reads as: for $t \in (0, T]$ find $p'(\mathbf{x}, t) \colon \Omega_0 \times (0, T] \to \mathbb{R}$ such that

$$\frac{1}{c_0^2} \frac{\partial^2 p'}{\partial t^2} - \Delta p' = \begin{cases} \nabla \cdot \nabla \cdot (\rho_0 \, \mathbf{u} \otimes \mathbf{u}) & \text{in } \Omega_1 \times (0, T] \ , \\ 0 & \text{in } \Omega_0 \setminus \Omega_1 \times (0, T] \ , \end{cases} \tag{11}$$

and which satisfies the following boundary and initial conditions

$$\begin{aligned} \frac{\partial p'}{\partial \mathbf{n}} &= 0 && \text{on } \Gamma_\mathrm{b} \times (0, T] \, , \\ \frac{\partial p'}{\partial \mathbf{n}} &= -\frac{1}{c_0} \frac{\partial p'}{\partial t} && \text{on } \Gamma_0 \times (0, T] \ , \\ p'(\mathbf{x}, 0) &= 0 && \text{for } \mathbf{x} \in \Omega_0 \, , \\ \frac{\partial p'}{\partial t}(\mathbf{x}, 0) &= 0 && \text{for } \mathbf{x} \in \Omega_0 \, , \end{aligned} \tag{12}$$

where $\mathbf{n}$ is the outward unit vector to Γ_b and Γ_0.

The acoustic sources $\nabla \cdot \nabla \cdot (\rho_0 \, \mathbf{u} \otimes \mathbf{u})$ within the near-field domain Ω_1 are evaluated using the fluid velocity $\mathbf{u}$ obtained from the Navier-Stokes equations for incompressible fluid, see eq. (5). Non-reflective boundary condition is prescribed in eq. (12) on the boundary Γ_0 to mitigate acoustic reflections.

3. Finite volume discretization

The discretization of eq. (5) involves subdivision of the domain Ω_1 into a finite number of closed, non-overlapping polygonal cells V_k (with volume $|V_k|$), such that $\Omega_1 = \bigcup_{k \in \mathcal{J}} V_k$, where $\mathcal{J}$ is an index set. Integrating eq. (5) over an arbitrary polygon V_k yields

$$\begin{aligned} \int_{V_k} \frac{\partial \mathbf{u}}{\partial t} \, \mathrm{d}V + \int_{V_k} \nabla \cdot (\mathbf{u} \otimes \mathbf{u}) \, \mathrm{d}V - \int_{V_k} \nabla \cdot (\nu \nabla \mathbf{u}) \, \mathrm{d}V + \int_{V_k} \frac{1}{\rho_0} \nabla p \, \mathrm{d}V = \mathbf{0} \,, \\ \int_{V_k} \nabla \cdot \mathbf{u} \, \mathrm{d}V = 0 \,. \end{aligned} \tag{13}$$

The solution of (13) is approximated by piecewise constant functions $\mathbf{u}_k, p_k$ given as

$$\mathbf{u}_k \approx \frac{1}{|V_k|} \int_{V_k} \mathbf{u} \, \mathrm{d}V \,, \quad p_k \approx \frac{1}{|V_k|} \int_{V_k} p \, \mathrm{d}V \,.$$

Considering V_k remains constant over time, the time derivative of velocity in eq. (13) can be cast in form $\int_{V_k} \partial \mathbf{u}/\partial t \, \mathrm{d}V \approx |V_k| \, \mathrm{d}\mathbf{u}_k/\mathrm{d}t$. For the time discretization, we first divide the temporal interval $(0, T]$ into N subintervals, such that $T = N\Delta t$, setting $t^n = n\Delta t$, with $n = 0, \ldots, N$, where Δt denotes constant time step. The Crank-Nicolson scheme is used for the temporal dicretization in the form

$$\frac{\mathrm{d}\mathbf{u}_k}{\mathrm{d}t} \approx \left[\frac{1}{1 + c_{\mathrm{oc}}} \left(\frac{\mathbf{u}_k^{n+1} - \mathbf{u}_k^n}{\Delta t} \right) - \frac{c_{\mathrm{oc}}}{1 + c_{\mathrm{oc}}} \left(\frac{\mathbf{u}_k^n - \mathbf{u}_k^{n-1}}{\Delta t} \right) \right], \tag{14}$$

where c_{oc} is an off-centering coefficient, see [6]. For $c_{\mathrm{oc}} = 0$ the scheme results in the implicit Euler scheme, whereas for $c_{\mathrm{oc}} = 1$ the central scheme is obtained. In the following work, $c_{\mathrm{oc}} = 0.9$ is used.

For other terms in eq. (13), we employ Gauss's theorem and approximate them using the midpoint quadrature rule on the face $f \in S_k$, where S_k is the set of all faces of the cell V_k and $|S_f|$ denotes the surface of face f, as

$$\int_{V_k} \nabla \cdot (\mathbf{u} \otimes \mathbf{u}) \, \mathrm{d}V = \oint_{\partial V_k} \mathbf{u} \, (\mathbf{u} \cdot \mathbf{n}) \, \mathrm{d}S \approx \sum_{f \in S_k} \mathbf{u}_f \, (\mathbf{u}_f \cdot \mathbf{s}_f) = \sum_{f \in S_k} \mathbf{u}_f \, \phi_f \,, \tag{15}$$

$$\int_{V_k} \nu \Delta \mathbf{u} \, \mathrm{d}V = \oint_{\partial V_k} \nu \, (\nabla \mathbf{u}) \cdot \mathbf{n} \, \mathrm{d}S \approx \nu \sum_{f \in S_k} (\nabla \mathbf{u})_f \cdot \mathbf{s}_f \,, \tag{16}$$

$$\int_{V_k} \frac{1}{\rho_0} \nabla p \, \mathrm{d}V = \oint_{\partial V_k} \frac{1}{\rho_0} (p \, \mathbf{I}) \cdot \mathbf{n} \, \mathrm{d}S \approx \frac{1}{\rho_0} \sum_{f \in S_k} (p_f \, \mathbf{I}) \cdot \mathbf{s}_f \,, \tag{17}$$

where $\mathbf{s}_f = \mathbf{n}\,|S_f|$ and $\phi_f = \mathbf{u}_f \cdot \mathbf{s}_f$ represents the volumetric flux at face f. The continuity equation in (13) enforces the sum of fluxes across all faces to be zero, i.e. $\sum_{f \in S_k} \phi_f = 0$ in order to satisfy the divergence-free condition. Concerning the discretization of the fluxes in (15)–(17) and the gradient reconstruction of velocity in eq. (16) we refer to [6].

For solving the discretized NSE for incompressible fluid, the PIMPLE algorithm is used as a combination of SIMPLE (semi-implicit method for pressure-linked equations) and PISO (pressure-implicit algorithm with the splitting of the operator). We begin by discretizing the momentum equation (13). Let $a_C^{\mathbf{u}}$ and $a_N^{\mathbf{u}}$ represent the coefficients in the resulting algebraic equations, where C and N refer to the central and neighboring cells, respectively. The discretized momentum equation then reads

$$a_C^{\mathbf{u}}\mathbf{u}_C + \sum_{f \in S_k} a_N^{\mathbf{u}}\mathbf{u}_N = \mathbf{r} - \frac{1}{\rho_0}(\nabla p)_C\,, \tag{18}$$

where vector $\mathbf{r}$ represents contributions from previous time steps. Next we introduce operator $\mathbf{H}(\mathbf{u}) = \mathbf{r} - \sum_{f \in S_k} a_N^{\mathbf{u}}\mathbf{u}_N$ such that

$$\mathbf{u}_C = (a_C^{\mathbf{u}})^{-1}\left[\mathbf{H}(\mathbf{u}) - \frac{1}{\rho_0}(\nabla p)_C\right]\,. \tag{19}$$

We substitute eq. (19) into the continuity equation to obtain a pressure equation

$$\nabla \cdot \left[(a_C^{\mathbf{u}})^{-1}(\nabla p)_C\right] = \rho_0 \nabla \cdot \left[(a_C^{\mathbf{u}})^{-1}\mathbf{H}(\mathbf{u})\right]\,. \tag{20}$$

The PIMPLE algorithm is based on a predictor and corrector step. In the predictor step, we solve eq. (18) using an intermediate pressure to obtain predicted velocity, which does not yet satisfy the continuity equation. We follow with the corrector step, in which we solve eq. (20) to obtain corrected pressure, and subsequently divergence-free velocity is obtained from eq. (19). We repeat these inner and outer loops until the pressure and velocity fields converge, see [6] for further reference. Additionally, under-relaxation can be used in each time step to smooth convergence.

4. Finite element discretization

In order to approximate the inhomogeneous wave equation (11) using FEM, the equation is multiplied by a test function $w \in \mathcal{V} \subset H^1(\Omega_0)$ and integrated over the entire acoustic domain Ω_0. This yields

$$\frac{1}{c_0^2}\left(\frac{\partial^2 p'}{\partial t^2}, w\right)_{\Omega_0} - (\Delta p', w)_{\Omega_0} = (\nabla \cdot \nabla \cdot (\rho_0\,\mathbf{u} \otimes \mathbf{u})\,, w)_{\Omega_0}\,, \tag{21}$$

where by $(\cdot,\cdot)_D$ the dot product in $L_2(D)$ is denoted. After applying Green's integration theorem to the second spatial derivate of p' as well as to the acoustic source

term on the right-hand side, the eq. (21) can be rearranged into

$$\begin{aligned}\frac{1}{c_0^2}\left(\frac{\partial^2 p'}{\partial t^2}, w\right)_{\Omega_0} - \left(\frac{\partial p'}{\partial \mathbf{n}}, w\right)_{\partial\Omega_0} + (\nabla p', \nabla w)_{\Omega_0} \\ = (\nabla\cdot(\rho_0\,\mathbf{u}\otimes\mathbf{u})\cdot\mathbf{n}, w)_{\partial\Omega_1} - (\nabla\cdot(\rho_0\,\mathbf{u}\otimes\mathbf{u}), \nabla w)_{\Omega_1}\,.\end{aligned} \tag{22}$$

Boundary conditions are applied to each boundary term. For the source term in eq. (22), this leads to the condition $(\nabla\cdot(\rho_0\,\mathbf{u}\otimes\mathbf{u})\cdot\mathbf{n}, w)_{\partial\Omega_1} = 0$ since

$$\begin{aligned}(\nabla\cdot(\rho_0\,\mathbf{u}\otimes\mathbf{u})\cdot\mathbf{n}, w)_{\Gamma_1} &= 0\,,\\ (\nabla\cdot(\rho_0\,\mathbf{u}\otimes\mathbf{u})\cdot\mathbf{n}, w)_{\Gamma_b} &= 0\,,\end{aligned} \tag{23}$$

for details, see [2]. This leads to the variational (weak) formulation of Lighthill's aeroacoustic equation, which may be stated as: find $p' \in \mathcal{V}$ such that

$$\frac{1}{c_0^2}\left(\frac{\partial^2 p'}{\partial t^2}, w\right)_{\Omega_0} + \frac{1}{c_0}\left(\frac{\partial p'}{\partial t}, w\right)_{\Gamma_0} + \left(\frac{\partial p'}{\partial x_i}, \frac{\partial w}{\partial x_i}\right)_{\Omega_0} = -(\nabla\cdot(\rho_0\,\mathbf{u}\otimes\mathbf{u}), \nabla w)_{\Omega_1}\,, \tag{24}$$

is fulfilled for all $w \in \mathcal{V}$. The source term in eq. (24) can be further simplified for incompressible fluid flows as follows

$$(\nabla\cdot(\rho_0\,\mathbf{u}\otimes\mathbf{u}), \nabla w)_{\Omega_1} = \rho_0\,(\mathbf{u}\cdot\nabla\mathbf{u}, \nabla w)_{\Omega_1}\,. \tag{25}$$

The semi-discrete Galerkin formulation is obtained from the weak formulation (24) after discretization of the domain and the introduction of finite element spaces. A finite-dimensional finite element space $V_h \subset \mathcal{V}$ with dimension n is chosen and the solution $p' \in \mathcal{V}$ is approximated by $p_h \in V_h$ written as a time-dependant linear combination of coefficients $p_j(t)$ and basis functions $\varphi_j(x) \in V_h$, i.e.

$$p'(x,t) \approx p_h(t,x) = \sum_{j=1}^{n} p_j(t)\varphi_j(x)\,. \tag{26}$$

Using relation (26) in eq. (24) with $w_h = \varphi_i$ for $i = 1, \ldots, n$ leads to the second-order system of ODEs for an unknown vector $\mathbf{p}(t) = \{p_j\}_{j=1}^n$ in the matrix form

$$\frac{1}{c_0^2}\mathbb{M}\ddot{\mathbf{p}}(t) + \frac{1}{c_0}\mathbb{D}\dot{\mathbf{p}}(t) + \mathbb{K}\mathbf{p}(t) = \mathbf{b}(t)\,, \tag{27}$$

where the matrices $\mathbb{M} = \{m_{ij}\}_{i,j=1}^n, \mathbb{D} = \{d_{ij}\}_{i,j=1}^n$ $\mathbb{K} = \{k_{ij}\}_{i,j=1}^n$ and the vector $\mathbf{b} = \{b_i\}_{i=1}^n$ are computed as follows

$$m_{ij} = (\varphi_j, \varphi_i)_{\Omega_0}\,, \quad d_{ij} = (\varphi_j, \varphi_i)_{\Gamma_0}\,, \quad k_{ij} = \left(\frac{\partial\varphi_j}{\partial x_l}, \frac{\partial\varphi_i}{\partial x_l}\right)_{\Omega_0}\,,$$

$$b_i = -\rho_0\left(u_l\frac{\partial u_j}{\partial x_l}, \frac{\partial\varphi_i}{\partial x_j}\right)_{\Omega_1}\,.$$

The problem described in eq. (27) is discretized in time with the aid of the Newmark method. This method is formally realized by using approximations

$$\begin{aligned} \mathbf{p}_{n+1} &= \mathbf{p}_n + \dot{\mathbf{p}}_n \, \Delta t + ((1-2\beta)\ddot{\mathbf{p}}_n + 2\beta\ddot{\mathbf{p}}_{n+1}) \, \frac{\Delta t^2}{2} \,, \\ \dot{\mathbf{p}}_{n+1} &= \dot{\mathbf{p}}_n + ((1-\gamma)\ddot{\mathbf{p}}_n + \gamma\ddot{\mathbf{p}}_{n+1}) \, \Delta t \,, \end{aligned} \tag{28}$$

in eq. (27), which is solved for $\ddot{\mathbf{p}}_{n+1}$. Values β and γ are taken as $\beta = 0.25$, $\gamma = 0.5$.

5. Implementation

The finite volume approach available within the OpenFOAM library has been adopted for space and time discretization of the NSE for incompressible fluid. Tab. 1 briefly describes the basic directory structure for OpenFOAM case that is required to run the simulation. The exception is the acousticMesh and funcObjects folders, which include the neccessary data for evaluation of the acoustic sources within the fluid domain and their subsequent interpolation onto the acoustic domain.

0	→ Initial and boundary conditions for fields
⌞ U	
⌞ p	
constant	
⌞ transportProperties	→ Physical properties of the fluid
⌞ turbulenceProperties	→ Type of fluid flow
⌞ polyMesh	→ Mesh data for the fluid domain
⌞ acousticMesh	→ Mesh data for the acoustic domain
system	
⌞ controlDict	→ Simulation's control parameters
⌞ fvSchemes	→ Numerical schemes used for discretizing
⌞ fvSolution	→ Solver settings and relaxation factors
⌞ funcObjects	→ Custom functions to be applied during
⌞ ...	simulation

Table 1: OpenFOAM folder structure.

Once the fluid simulation is finished and the acoustic sources have been interpolated for the desired time period, the Lighthill's aeroacoustic equation is solved using the FEM framework implemented in the FEniCS Python library (see [1]).

After importing the acoustic mesh in *.msh* format, a finite element function space V is created. The trial function p and test function w are then defined, followed by the initialization of fem.Function, which stores the coefficients for the solution.

```
from dolfinx import fem, import ufl
V = fem.functionspace(msh, ("Lagrange", 1))
p, w = ufl.TrialFunction(V), ufl.TestFunction(V)
p_h = fem.Function(V)
```

Similarly, we initalize fem.Function for the divergence of Lighthill's tensor.

```
V_divT = fem.functionspace(msh, ("Lagrange", 1, (msh.geometry.dim,)))
divT = fem.Function(V_divT)
```

We also prepare data structures for the Newmark method.

```
p_0, pdot_0, pddot_0 = fem.Function(V), fem.Function(V), fem.Function(V)
pddot = p
pdot = pdot_0 + ((1-gamma)*pddot_0 + gamma*pddot) * dt
p_ = p_0 + pdot_0*dt + ((1-2*beta)*pddot_0 + 2*beta*pddot) * dt**2/2
```

The integration measures are defined to substitute for the different subdomain cells and their boundary faces.

```
ds = ufl.Measure("ds", domain=msh, subdomain_data=boundary_tags)
dx = ufl.Measure("dx", domain=msh, subdomain_data=subdomain_tags)
```

With all the data structures in place, we define the variational formulation.

```
F = 1 / c_0**2 * ufl.inner(pddot, w) * dx(0) \
    + 1 / c_0 * ufl.inner(pdot, w) * ds(0) \
    + ufl.inner(ufl.grad(p_), ufl.grad(w)) * dx(0) \
    + ufl.inner(divT, ufl.grad(w)) * dx(1)
a, L = ufl.system(F)
```

Using the finite element variational problem formulation, the class dolfinx.fem.petsc.LinearProblem is created for solution of the variational problem. This class utilizes PETSc as the linear algebra backend and a direct solver (LU-factorization) is employed to solve the linear system.

```
import dolfinx.fem.petsc
problem = dolfinx.fem.petsc.LinearProblem(a, L, u=p_h, bcs=[], petsc_options)
```

Finally, the problem is solved repeatedly in time in order to obtain the evolution of the acoustic pressure field.

```
t = t_start
while t < t_end + dt:
    divT = get_interpolated_OpenFOAM_field(divT, msh, t)
    p_h = problem.solve()
    p_0, pdot_0, pddot_0 = evaluate_Newmark_fields(p_h, p_0, pdot_0, pddot_0)
    write_results(p_0, t)
    t += dt
```

6. Numerical results

A laminar, two-dimensional simulation of an incompressible fluid flow over a square cylinder is performed. When a rigid square cylinder is immersed in a uniform flow, it generates strong vortex shedding. The resulting fluctuating forces on the cylinder induce acoustic waves, which are the focus of this study.

By $L_{\text{cyl}} = 3.28 \cdot 10^{-5}$ m we denote the dimension of the cylinder. The dimensions of the fluid computational domain Ω_1 are then (-$30L_{\text{cyl}}$, $100L_{\text{cyl}}$) $\times$ ($-25L_{\text{cyl}}$, $25L_{\text{cyl}}$), with a blockage ratio[1] of $\beta = L_{\text{cyl}}/50L_{\text{cyl}}$. The acoustic domain Ω_0 is a circle with a radius of $150L_{\text{cyl}}$. The mesh within the fluid domain is roughly three times finer than the mesh for the acoustic simulation, as can be seen in Fig. 3. The flow properties and the setup of the simulation are listed in Tab 2. The fluid flow

[1]The ratio of the square cylinder's frontal area to the domain's cross-sectional area in the flow direction.

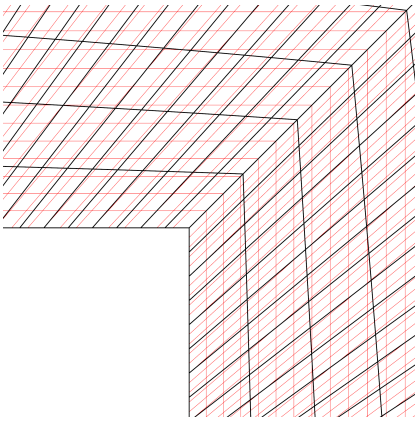

Figure 3: Acoustic (black) and fluid (red) mesh near cylinder.

Setup of the simulation		
U_∞	=	68.7 m s^{-1}
L_{cyl}	=	$3.28 \cdot 10^{-5}$ m
ν	=	$1.5 \cdot 10^{-5}$ $m^2 s^{-1}$
c_0	=	343 m s^{-1}
ρ_0	=	1.2 kg m^{-3}
Re	=	150
Ma	=	0.2

Table 2: Setup of the simulation.

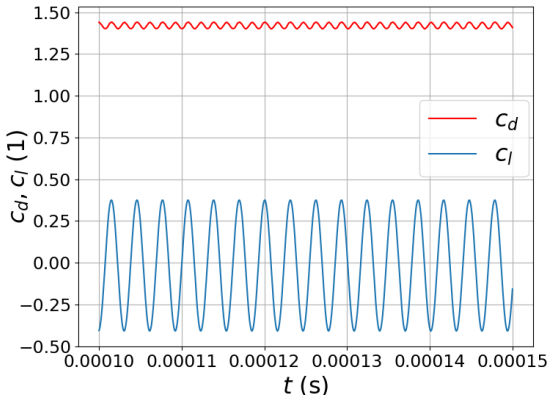

Figure 4: Lift and drag coefficients in time.

	$\overline{c_D}$	St
present study	1.42	0.153
Doolan [3]	1.44	0.156

Table 3: Comparison of the mean drag coeffcient and Strouhal number with reference values.

solution is sampled after the full vortex street developed from $t_0^{\text{a}} = 1 \cdot 10^{-4}$ s every 10 fluid time steps, i.e. $\Delta t^{\text{a}} = 10^{-8}$ s and $\Delta t^{\text{f}} = 10^{-9}$ s, until the end of simulation $t_{\text{end}} = 1.5 \cdot 10^{-4}$ s. The whole time of acoustic simulation is $0.5 \cdot 10^{-4}$ s. The lift and drag coefficients are plotted in time in Fig. 4. The mean drag coefficient $\overline{c_D}$ and Strouhal number St based on vortex shedding frequency are evaluated and compared to reference values with good agreement, see Tab. 3. The acoustic pressure values are monitored at three different observer locations. The first two observers are positioned downstream along the x-axis and along the fringe of the cylinder, respectively. Significantly lower values are anticipated at the third observer location in the far-field region, see Tab. 4. Fig. 5 presents the acoustic field (scaled by dynamic pressure) at final time, in which dipole pattern can be seen. The acoustic pressure values at three observer locations are shown in Fig. 6 in the time and frequency domain. The main frequency component for observer 2 and 3 corresponds to the vortex shedding frequency. On the other hand, the main frequency component for observer 1, located along the x-axis is twice as high. This fact can be associated with the combination of the upper and lower vortices.

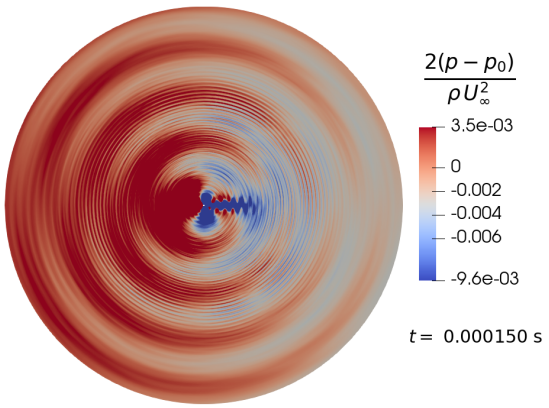

Figure 5: Acoustic pressure field.

Observers	
1:	$(1 \cdot 10^{-4}, 0, 0)$ m
2:	$(1 \cdot 10^{-4}, 2 \cdot 10^{-5}, 0)$ m
3:	(0.002, -0.003, 0) m

Table 4: Positions of the observers with respect to the origin of the coordinate system located in the center of the square cylinder.

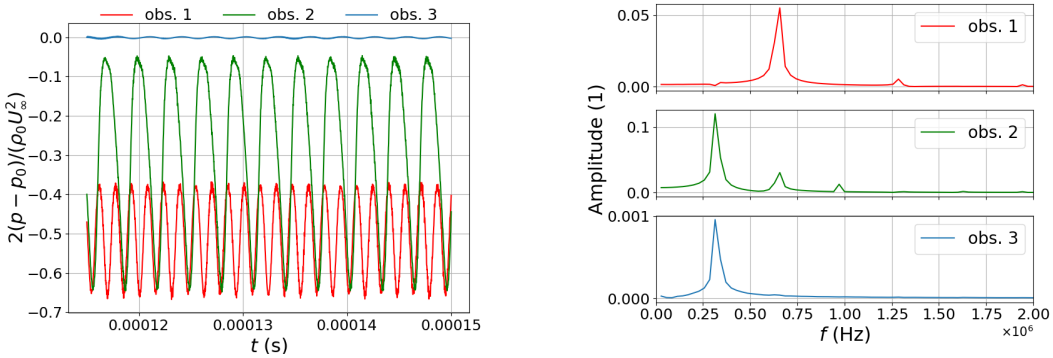

Figure 6: Acoustic pressure at three observer locations in: (a) the time domain and (b) the frequency domain.

7. Conclusion

In this study we have adopted a hybrid method for CAA that establishes a foundation for future aeroacoustic investigations. Our primary focus was on a 2D square cylinder placed within a laminar flow with Reynolds number 150 and Mach number 0.2. The presence of the square cylinder resulted in the formation of strong vortices in the downstream region, which induced acoustic waves. The resulting acoustic pressure obtained by Lighthill's aeroacoustic analogy was analyzed both in the near-field and far-field acoutic region. The dominant frequencies for selected observers correspond with expectations.

Acknowledgements

This work was supported by the Czech Technical University in Prague under the grant No. SGS24/120/OHK2/3T/12 and grant No. SGS22/148/OHK2/3T/12. The authors also gratefully acknowledge the Center of Advanced Aerospace Technology (CZ.02.1.01/0.0/0.0/16_019/0000826) at the Czech Technical University in Prague for awarding the access to computing facilities.

References

[1] Baratta, I. A. et al.: DOLFINx: The next generation FEniCS problem solving environment, 2023.

[2] Caro, S., Ploumhans, P., and Gallez, X.: Implementation of lighthill's acoustic analogy in a finite/infinite elements framework. 10th AIAA/CEAS Aeroacoustics Conference, (2004).

[3] Doolan, C. J.: Flat-plate interaction with the near wake of a square cylinder. AIAA Journal **47** (2009), 475–479.

[4] Ewert, R. and Schröder, W.: Acoustic perturbation equations based on flow decomposition via source filtering. J. Comput. Phys. **188** (2003), 365–398.

[5] Lighthill, M. J.: On sound generated aerodynamically. i. general theory. Proceedings of the Royal Society of London. Series A, Mathematical and Physical Sciences **211** (1952), 564–587.

[6] Moukalled, F., Mangani, L., and Darwish, M.: *The finite volume method in computational fluid dynamics: an advanced introduction with OpenFOAM and Matlab*. Springer International Publishing, Cham, 2016.

[7] Schoder, S. and Kaltenbacher, M.: Hybrid aeroacoustic computations: State of art and new achievements. J. Theor. Comput. Acoust. **27** (2019).

[8] Valášek, J. and Sváček, P.: Aeroacoustic simulation of human phonation based on the flow-induced vocal fold vibrations including their contact. Adv. Eng. Softw. **194** (2024).